Ultramicroscopy 182 (2017) 81–84

Contents lists available at ScienceDirect

Ultramicroscopy

journal homepage: www.elsevier.com/locate/ultramic

An aperture design for single side band imaging in the transmission electron microscope

Philip J.B. Koeck

Royal Institute of Technology, School of Technology and Health and Karolinska Institutet, Department of Biosciences and Nutrition, Novum, 14183 Huddinge, Sweden

ARTICLE INFO

Article history:
Received 14 March 2017
Revised 26 April 2017
Accepted 18 June 2017
Available online 22 June 2017

Keywords:
Single side band imaging
Single side band objective aperture
Weak phase object approximation
Transfer function
Transmission electron microscopy

1. Introduction

In theory single side band or Schlieren imaging could be a promising method for imaging low contrast specimens in the transmission electron microscope. However, it has so far not been applied very much in this field [1]. Technical problems that have been pointed out are the charging of the aperture edge [2,3] and the difficulty of determining defocus and astigmatism from the images [1]. Buijsse [4] has suggested an aperture design that allows recording images at approximate Scherzer defocus in such a way that the lowest spatial frequencies are imaged using the single side band method whereas higher spatial frequencies are imaged as regular (or double side band) phase contrast. This allows determination of defocus and astigmatism from the Thon rings visible at the higher spatial frequencies. This information can then be used to correct for the phase errors introduced to the low frequency part of the image as well as the contrast inversion at high spatial frequencies.

In this paper I suggest an aperture design which allows determining defocus and astigmatism for images recorded in single side band mode at all spatial frequencies without the choice of a particular defocus. The aperture should work equally well for recording images at Scherzer defocus and several hundred nanometers under-focus. The key to this lies in the three "gaps" in Fourier space where Fourier components pass through the aperture as Friedel pairs. As a consequence, Thon rings are visible in these gaps and allow for correction of defocus and astigmatism in the entire spatial frequency range (see Figs. 1 and 2 and the theory section). Charging of the aperture edge can be limited by keeping a distance to the primary beam with the obvious drawback that the lowest spatial frequencies will be imaged with defocusing contrast rather than single side band contrast.

In the following I present an image formation theory for imaging weak phase objects using the suggested aperture and a method of correcting for the resulting transfer function. I test both the image formation theory and the correction method in computer simulations.

2. Single side band imaging – theory and simulations

For a weak phase object the Fourier transform of the exit wave $\Psi_{ex}(\vec{u})$ is modified by the objective lens and side band aperture as follows:

$$\Psi_{pc}\left(\vec{u}\right) = \Psi_{ex}\left(\vec{u}\right) e^{-i\,\chi\left(\vec{u}\right)} H\left(\vec{u}\right) \approx \left[\delta\left(\vec{u}\right) + i\,\sigma\,F\left(\vec{u}\right)\right] e^{-i\,\chi\left(\vec{u}\right)} H\left(\vec{u}\right) \quad (1)$$

Here $\chi(\vec{u})$ is the lens aberration function including defocus, spherical aberration and astigmatism and $H(\vec{u})$ is a binary function describing the effect of the aperture as depicted in Fig. 2A.

Abbreviations: TEM, transmission electron microscopy/microscope; 3D, three-dimensional; POA, phase object approximation.

E-mail address: philip.koeck@ki.se

http://dx.doi.org/10.1016/j.ultramic.2017.06.018

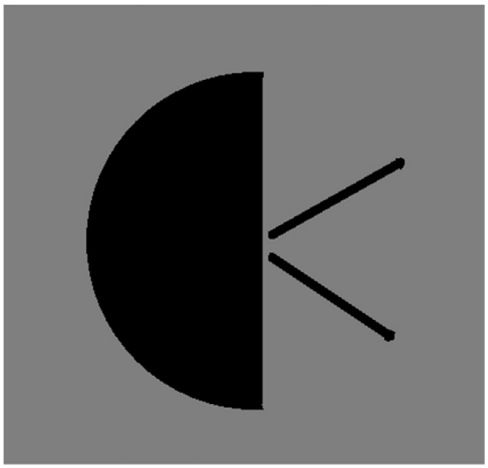

Fig. 1. Suggestion for a single side band aperture. The outer diameter should be chosen such as not to limit the highest expected resolution for a given microscope and type of specimen and could be in the order of 50 to 100 µm. The straight edge is slightly off-center to allow the primary beam to pass and the two slits can have a width in the order of 5 µm such that Thon rings become clearly visible in the corresponding areas of the image's Fourier transform (see Fig. 2).

The exit wave in real space is given by

$$\Psi_{ex}\left(\vec{x}\right) = e^{i\ \sigma\ proj\left(\vec{x}\right)} \approx 1 + i\ \sigma\ proj\left(\vec{x}\right) \tag{2}$$

Variables in real and Fourier space are two-dimensional so that $\vec{x} = \binom{x}{y}$ and $\vec{u} = \binom{u_x}{u_y}$.

σ is the interaction constant, $\sigma = \frac{2\pi m e \lambda_i}{h^2}$.

$F(\vec{u})$ is the Fourier transform of $proj(\vec{x})$ and $proj(\vec{x})$ is the projection of the electrostatic potential distribution along the z-axis.

Using the Hermitian property of $F(\vec{u})$ and the inversion symmetry of $\chi(\vec{u})$ (plus a change of sign in the integration variables of one of the integrals) the image then becomes:

$$\begin{aligned} im_{pc}\left(\vec{x}\right) &= \psi_{pc}\left(\vec{x}\right)\ \psi^*_{pc}\left(\vec{x}\right) \\ &\approx \left[1 + i\ \sigma \int F\left(\vec{u}\right)\ H\left(\vec{u}\right) e^{-i\ \chi\left(\vec{u}\right)}\ e^{2\pi i \vec{x}\ \vec{u}}\ du_x du_y\right] \\ &\quad \cdot \left[1 - i\ \sigma \int F^*\left(\vec{u}\right)\ H\left(\vec{u}\right) e^{i\chi\left(\vec{u}\right)}\ e^{-2\pi i \vec{x}\ \vec{u}}\ du_x du_y\right] \\ &= \left[1 + i\ \sigma \int F\left(\vec{u}\right)\ H\left(\vec{u}\right) e^{-i\chi\left(\vec{u}\right)}\ e^{2\pi i \vec{x}\ \vec{u}}\ du_x du_y\right] \\ &\quad \cdot \left[1 - i\ \sigma \int F\left(\vec{u}\right)\ H\left(-\vec{u}\right) e^{i\ \chi\left(\vec{u}\right)}\ e^{2\pi i \vec{x}\ \vec{u}}\ du_x du_y\right] \end{aligned}$$

The last line of the above derivation can be approximated by the following expression (excluding the quadratic term):

$$\begin{aligned} im_{pc}\left(\vec{x}\right) \approx 1 + \sigma \int F\left(\vec{u}\right) \left[i\ H\left(\vec{u}\right) e^{-i\chi\left(\vec{u}\right)} - i\ H\left(-\vec{u}\right) e^{i\chi\left(\vec{u}\right)}\right] \\ \times e^{2\pi i \vec{x}\ \vec{u}}\ du_x du_y \end{aligned} \tag{3}$$

The transfer function in Eq. (3) is in general complex valued. However, for all Fourier components where both $H(\vec{u})$ and $H(-\vec{u})$ are equal to 1 the two terms combine to the familiar real-valued $sin(\chi(\vec{u}))$ of bright-field phase contrast imaging. This effect can be seen in Fig. 2D. It is important to realize that outside the "gaps" the transfer function is complex valued with a modulus of 1 and thus does not down-weight any spatial frequencies.

To correct for the effects of this transfer function on the image one simply needs to multiply the Fourier transform of the image by the complex conjugate of the term in square brackets in Eq. (3) and then back-transform.

In the simulation of the image shown in Fig. 2C I used a weak phase object (see [5] for approximate phase shifts) as input, but I did not use the weak phase approximation for calculating the exit wave. Instead I calculated the exit wave using the exponential phase factor as given in Eq. (2) directly after the equal-sign. This was done in order to test the validity of the described image formation theory for weak phase objects.

The simulation procedure was the following:

The electrostatic potential distribution inside trypsin inhibitor (Protein data Bank entry 4pti), a small protein with a diameter of about 2.5–3 nm, was calculated using Matlab-code written by Shang and Sigworth. This code treats the molecule as a collection of neutral atoms as described in [6]. Each atom is assigned an atomic radius and a single potential value, obtained at the limit of low scattering angles from the parametrization of [7]. All further steps of phantom construction and electron microscopic imaging simulation were implemented in Khoros [8]. The phantoms used as specimens for image simulation were generated by arranging 6 copies of the electrostatic potential distribution in an asymmetric oligomer with a molecular mass of about 40 kDa.

All imaging simulations were done for a 300 kV microscope with a C_s of 2 mm. For this acceleration voltage the electron wave length becomes 0.002 nm and σ is 0.0065 rad / V nm.

The voxel size of the phantom and the pixel size of the projection and images are 0.5 Å, giving a Nyquist limit of 1 Å

When the electron wave travels down the column and hits the specimen it first enters a layer of vitrified water, which is modelled as a constant electrostatic potential distribution of about 4.9 V for all voxels occupied by water. In the vicinity of the protein the potential drops below this value to take into account the finite distance between water molecules and the atoms forming the surface of the protein. For details see [6].

The upper and lower surfaces of the water layer are assumed to be flat and orthogonal to the direction of the electron beam (z-axis).

The exit wave was calculated using Eq. (2) without approximating for weak phase objects. The specimen was treated as a single projection of the electrostatic potential since for the considered specimen thickness a multi-slice simulation gives results that are almost indistinguishable from simulations based on the projection assumption [5]. As shown in Eq. (1) the Fourier transform of the exit wave was then multiplied by the lens aberration function and the single side band aperture specified in Fig. 2. Partial spatial coherence of the electron source was taken into account by a Gaussian envelope with a standard deviation of 0.35 Nyquist in Fourier space. To arrive at an image the absolute square was taken in real space.

3. Simulation results

Fig. 2A shows the filter used to represent the aperture in the simulations. An image of the slightly noisy object shown in Fig. 2B is shown Fig. 2C. The Fourier transform of this image (Fig. 2D) clearly shows Thon rings in the "gaps" where Fourier components are imaged pair wise.

As described above the transfer function can be corrected by a simple multiplication in Fourier space leading to the corrected image shown in Fig. 3A with the object shown for comparison in Fig. 3B. This correction is relatively insensitive to errors in the defocus and astigmatism values in the order of about 10% and to a slight overestimation in the width of the gaps in Fourier space.